doi:10.1016/S0022-2836(03)00236-5 J. Mol. Biol. (2003) 328, 33–47

JMB

Available online at www.sciencedirect.com

SCIENCE DIRECT®

Understanding Discrimination by the Ribosome: Stability Testing and Groove Measurement of Codon–Anticodon Pairs

K. Y. Sanbonmatsu[1]* and S. Joseph[2]

[1]*Theoretical Biology and Biophysics Group Los Alamos National Laboratory, Los Alamos NM 87545, USA*

[2]*Department of Chemistry and Biochemistry University of California at San Diego, 9500 Gilman Drive, La Jolla, CA 92093 USA*

**Corresponding author*

The ribosome must discriminate between correct and incorrect tRNAs with sufficient speed and accuracy to sustain an adequate rate of cell growth. Here, we report the results of explicit solvent molecular dynamics simulations, which address the mechanism of discrimination by the ribosome. The universally conserved 16 S rRNA base A1493 and the kink in mRNA between A and P sites amplify differences in stability between cognate and near-cognate codon–anticodon pairs. Destabilization by the mRNA kink also provides a geometric explanation for the higher error rates observed for mismatches in the first codon position relative to mismatches in the second codon position. For more stable near-cognates, the repositioning of the universally conserved bases A1492 and G530 results in increased solvent exposure and an uncompensated loss of hydrogen bonds, preventing correct codon–anticodon–ribosome interactions from forming.

Published by Elsevier Science Ltd

Keywords: ribosome; molecular dynamics; translation; RNA; proofreading

Introduction

During translation, genetic information encoded by nucleic acid is used by the ribosome to synthesize protein. The ribosome must discriminate between correct and incorrect aminoacyl-tRNAs, accepting only those tRNAs whose anticodon is complementary to the mRNA codon in the aminoacyl site (A site) of the ribosome.[1–3] The exact molecular mechanism of discrimination has yet to be determined. In the kinetic proofreading model, discrimination occurs in two stages: initial selection and proofreading.[4–7] Initial selection is preceded by a distinct codon-independent binding step,[4,8] where the elongation factor EF-Tu brings the aminoacyl-tRNA to the ribosome in an aminoacyl-tRNA·GTP·EF-Tu ternary complex. The initial selection and proofreading stages are separated by hydrolysis of this GTP in the ternary complex.[4,7] The GTP hydrolysis and peptidyl transferase reactions are each preceded by rate-limiting conformational changes.[4,8] In the distortion detection model, the ribosome distinguishes between correct and incorrect tRNAs in a single step by measuring the geometry of the codon–anticodon minihelix.[9,10] In this model, codon–anticodon interactions at E site play an important role in modulating fidelity at site A.[11,12] It has recently been suggested that kinetic proofreading and distortion detection may occur simultaneously, with the ribosome detecting the correctness of the codon–anticodon pairing during both initial selection and proofreading.[13,14]

To fully understand the molecular mechanism of discrimination by the ribosome, one must examine the mechanism of rejection of near-cognate tRNA, in addition to the mechanism of acceptance of cognate tRNA. Cognate tRNAs are those whose anticodon matches the codon as prescribed by the genetic code. Near-cognate tRNAs usually have a single mismatch and their corresponding ternary complexes typically undergo several more rounds of GTP hydrolysis than cognates. The superb work of Ogle *et al*. has uncovered the mechanism of acceptance of cognate tRNA.[15] That is, the X-ray structure of the *Thermus thermophilus* small subunit complexed with a cognate $tRNA^{Phe}$ anticodon stem-loop analog (ASL^{Phe}) demonstrated that cognate recognition occurs *via* conformational changes of 16 S rRNA bases G530, A1492 and A1493, which bind across the codon–anticodon minihelix minor groove. Recently, X-ray structures

Abbreviations used: ASL, anticodon stem-loop; EM, electron microscopy.

E-mail address of the corresponding author: kys@lanl.gov

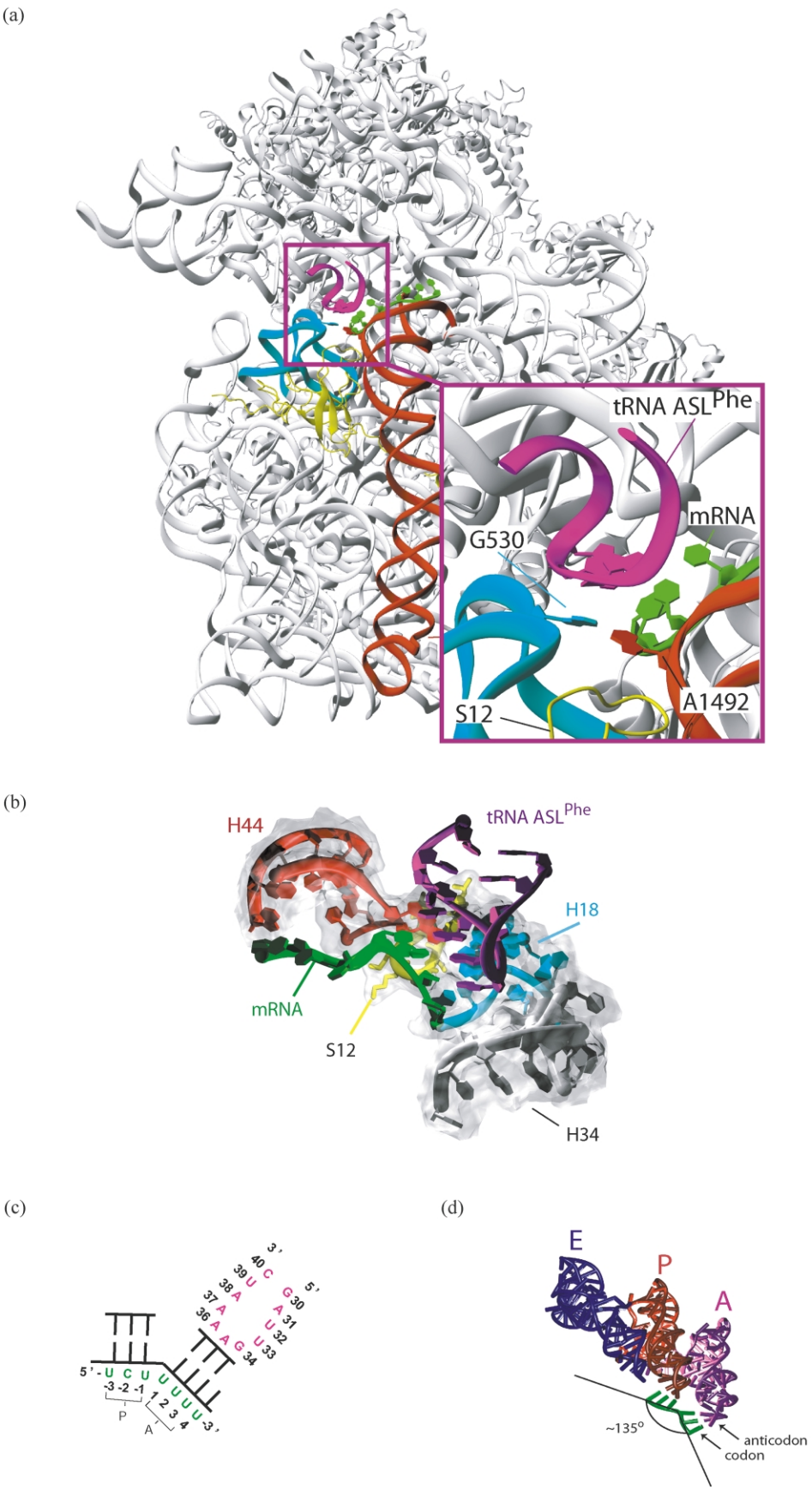

Figure 1 (*legend opposite*)

of the small subunit complexed with near-cognate ASLs have been determined, revealing that, while the small subunit undergoes a conformational change from an open to closed form upon cognate ASL binding, this same conformational change does not occur for near-cognate ASLs.[14] The near-cognate codon–anticodon–ribosome interactions, however, could not be resolved due to the disordered structure of the near-cognate ASLs, which bind only transiently to the ribosome. In an attempt observe these interactions, the error-inducing antibiotic paromomycin was soaked into the crystal. However, paromomycin functions by inducing the cognate tRNA–ribosome interactions, preventing the direct observation of near-cognate tRNA–ribosome interactions necessary to determine the molecular mechanism of discrimination. Here, we address this issue by performing all-atom explicit solvent molecular dynamics simulations of several near-cognate codon–anticodon–ribosome interactions in the absence of antibiotics. This approach is complementary to recent X-ray crystallography,[13–16] cryo-electron microscopy,[17,18] and kinetic studies[4] and helps establish a logical picture of the mechanism of discrimination.

While large-scale conformational changes are clearly important in the decoding process,[4,14,19] it is ultimately the interaction between codon and anticodon in the 30 S subunit A site which is responsible for the accuracy of translation. Therefore, here we have examined discrimination by investigating the local interactions at the ribosomal decoding center. This approach is justified for several reasons. First, tRNA bound to the ribosome in A/A and A/T states give identical footprints in 16 S rRNA.[20] Second, cryo-EM data suggests the local codon–anticodon–ribosome interactions at the decoding site in A/T and A/A states are similar.[17] Third, A site ASLs soaked into 30 S crystals have been used successfully as a model system to study the selection of cognate tRNA.[15] We use this model system as a basis for our work, which is relevant to both A/T and A/A states.

Discrimination between cognate and near-cognate codon–anticodon interactions may involve (1) sequence-dependent hydrogen bonding,[10] (2) steric fit,[10,11,13,21] and (3) base-pair stability. First, because each of the codon–anticodon–ribosome hydrogen bonds observed in the X-ray structure is sequence-independent,[15] discrimination based solely on sequence-dependent hydrogen bonding is unlikely. Second, it is not clear that steric fit (i.e. van der Waals interactions as opposed to hydrogen bonding) can be used to distinguish between Watson–Crick and non-Watson–Crick purine–pyrimidine pairs at the required rate because their minor grooves are composed of identical atoms. Third, although observed error rates cannot be achieved by discrimination based on base-pair stability alone,[22] discrimination may occur through the amplification of differences in stability between cognate and near-cognate codon–anticodon pairs by the ribosome.[23,24] Despite recent advances in understanding discrimination,[4,13,14] the relative contribution to discrimination by hydrogen bonding, steric fit, and base-pair stability is not well understood.

The molecular dynamics approach used here has previously helped elucidate functional mechanisms of other biomolecular systems[25–29] and has been validated against experiment.[30–32] Few researchers have attempted to address the ribosome discrimination problem using modeling approaches.[10,33,34] Rigid body docking and static models have been used to examine the codon–anticodon–ribosome interactions[10,33] and ternary complex initial selection.[34] Smaller scale molecular dynamics simulation studies of cognate codon–anticodon interactions in the absence of the ribosome have also been performed.[35] We have used molecular dynamics simulations to investigate the role of steric fit, hydrogen bonding and base-pair stability in discrimination by the ribosome. This study has also examined the question, why are error rates generally higher for first position mismatches than for second position mismatches?[22]

Results and Discussion

Simulations of the ribosomal decoding center

The high resolution structure of the 30 S-ASL^{Phe}–mRNA complex[15] was used as a basis for the simulations (Figure 1(a)). The simulation domain consists of those stretches of 16 S rRNA and a small subunit ribosomal protein which directly interact with the A site codon–anticodon pair, including bases 517–521 (H18), 527–533 (H18), 1052–1056(H34), 1194–1199 (H34), 1405–1410 (H44), 1490–1496 (H44), 30–40 (tRNA ASL^{Phe}), P site codon, A site codon, and residues 44–52 of ribosomal protein S12 (Figure 1(b) and (c)). The P site ASL was not included because simulations of cognate systems with A and P site ASLs exhibited similar results to those in absence of a P site ASL

Figure 1. Explicit solvent simulations of the codon–anticodon–ribosome interactions based on the 16 S rRNA–ASL^{Phe}–mRNA X-ray structure (RCSB PDB accession code 1IBM). (a) The 30 S X-ray structure showing tRNA–ASL^{Phe} (purple), messenger RNA (green), helix 18 (cyan), helix 44 (red), and protein S12 (yellow). The interaction between 16 S rRNA bases G530 and A1492 is shown in the inset. (b) The initial configuration of the cognate simulation domain, oriented to show the codon–anticodon interaction between the A site mRNA codon and tRNA–ASL^{Phe} anticodon. (c) Definition of mRNA sequence numbering for A and P site mRNA codons. (d) The structure of the A, P and E site tRNAs within the ribosome structure 1GIX[41] displays the kink in mRNA required for simultaneous A and P site codon–anticodon interactions.

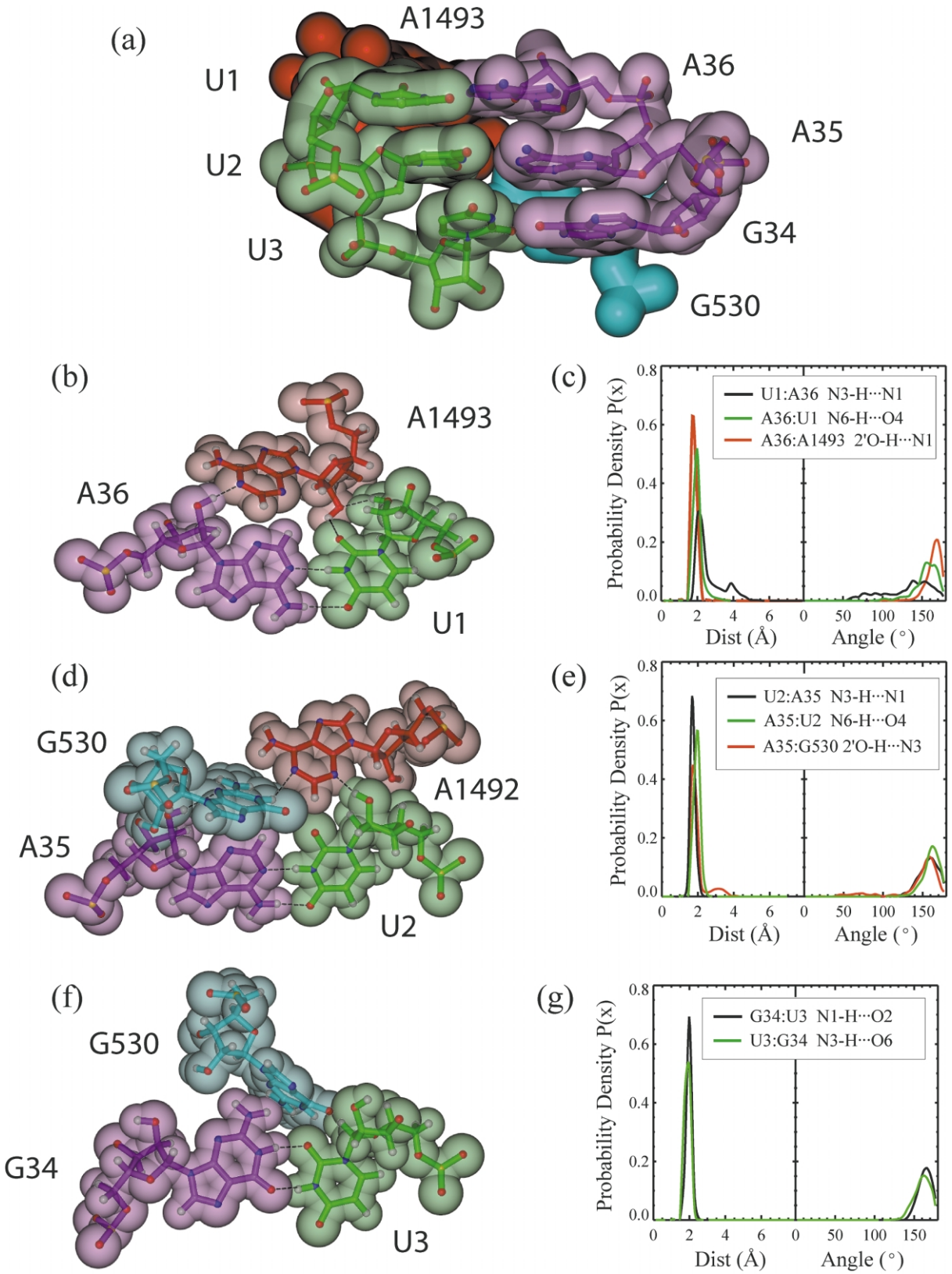

Figure 2. Cognate codon–anticodon–ribosome complex and the interactions for each codon–anticodon base-pair at late times (3.0 ns) during the simulation for UUU. This structure is a typical configuration of the 1.8×10^6 UUU configurations sampled. (a) codon–anticodon minihelix major groove. The 16 S rRNA bases A1492 (red), A1493 (red) and G530 (cyan) bind across the minor groove, seen in the background. (b) Codon position I, showing the A-minor motif[58,59] interaction between tRNA position A36 (purple), mRNA position U1 (green) and 16 S rRNA base A1493 (red). (c) Probability distributions of position I interactions involving the tRNA–ASL show stable hydrogen bonds with distances of <2.65 Å and angles $>$ 120°. (d) Codon position II interactions, showing the interaction between

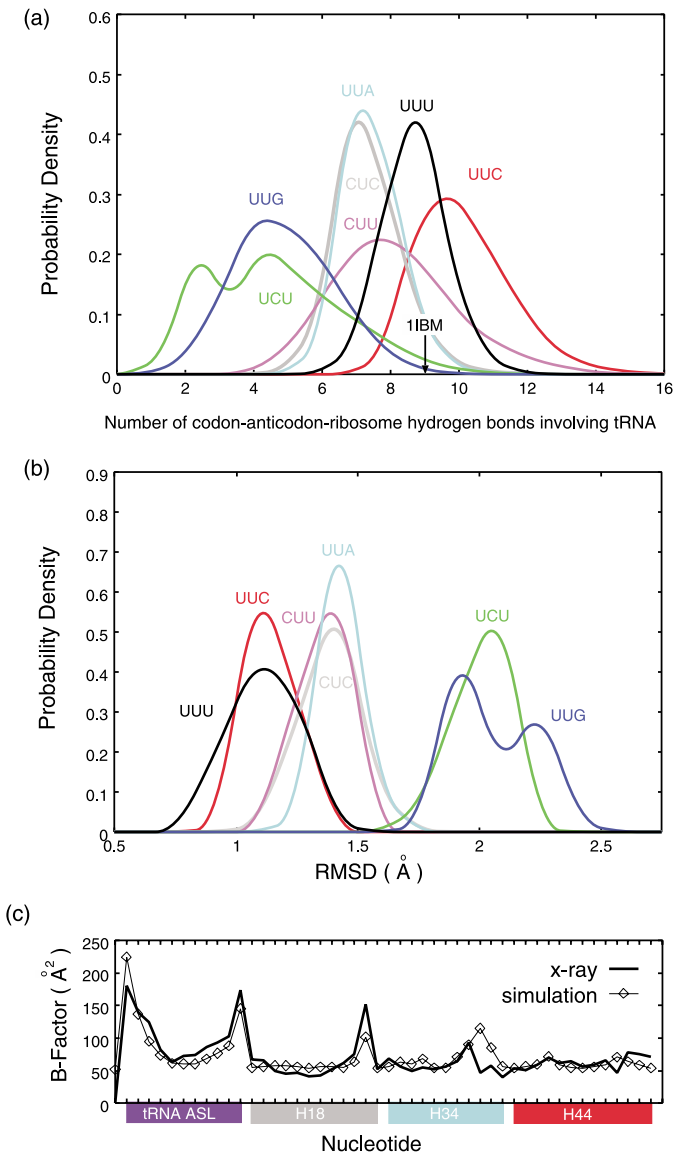

Figure 3. (a) Probability distributions of the number of codon–anticodon–ribosome hydrogen bonds involving the tRNA–ASL according to the criteria of distance $d < 2.65$ Å and angle $\theta > 120°$, where d is the D–H···A atom distance, θ is the D–H···A angle, D–H is the donor group, and A is the acceptor atom, consistent with the criteria used by Ogle *et al.*[15] (b) Probability distributions of the root-mean-squared deviation of the codon–anticodon–ribosome base structures (mRNA N1, N2, N3; tRNA G34, A35, A36; rRNA G530, A1492, A1493) from those of the X-ray structure (RCSB PDB accession code 1IBM). Distributions were smoothed using b-spline smoothing (see Methods). (c) Average RNA *B*-factors computed from the cognate UUU molecular dynamics simulation domain compared to those computed for the X-ray structure.

and displayed no interaction between A and P site ASLs. Instead, the P site codon was restrained to mimic the presence of the P site ASL. Each system was solvated with approximately 7×10^3 water molecules. A kink in the mRNA exists between A and P sites (Figure 1(d)). We have performed 20 3.0 ns molecular dynamics simulations (60.0 ns total sampling time of the decoding problem), including all codons differing from the cognate codon (UUU) by one base. As control simulations, we examined the cognate cases (UUU and UUC) as well as a non-cognate case with three mismatches (AAG), following the work described by Thompson.[7] To test the sensitivity of these results to the size of the simulation domain, additional simulations were performed including 16 S rRNA bases 912–916 and 1395–1404 in addition to the domain described above for cognate and near-cognate cases.

Cognate cases show stable codon–anticodon–ribosome interactions

The simulations for the cognate UUU codon produced stable codon–anticodon–ribosome hydrogen bonds, consistent with those observed in the crystal structure (Figure 2). The average number of codon–anticodon–ribosome hydrogen bonds involving the tRNA–ASL is $N_H \cong 8.70$, according to the criteria used by Ogle *et al.*, similar to the

G530 and A1492 across the minihelix minor groove. (e) Codon position II hydrogen bond distributions. (f) Codon position III interactions, showing the interaction between tRNA position G34 (purple), mRNA position U3 (green) and 16 S rRNA base G530 (cyan). (g) Codon position III hydrogen bond distributions.

value $N_H = 9$ observed in the crystal structure (Figure 3(a)). These hydrogen bonds have relatively low fluctuations, with hydrogen bond quality index (i.e. the deviation from Watson–Crick geometry hydrogen bonds, as defined in Methods) $I_H \cong 0.27$. The difference in number of hydrogen bonds between the simulation (8.70) and the X-ray structure (9.00) is due to the slightly higher fluctuations in the U1·A36 N3–H···N1 base-pair bond. Simulations with identical protocol were performed for the cognate UUC codon. This case (UUC) produced the most stable codon–anticodon interaction in our study, giving $I_H \cong 0.05$. The third position G·C pair in UUC forms three hydrogen bonds compared to the two bonds formed by the third position G·U wobble for UUU. Furthermore, the A35·G530 2′O–H···N3 and U1·A36 N3–H···N1 bonds satisfy the criteria for hydrogen bonding approximately 29% more often for UUC than UUU, resulting in an average number of codon–anticodon–ribosome hydrogen bonds of $N_H \cong 10.12$ for UUC (Figure 3(a)). The total number of codon–anticodon–ribosome hydrogen bonds involving the tRNA–ASL is greatest for the cognate cases (Figure 3(a); UUU and UUC) and the average root-mean-squared deviation (RMSD) away from the crystal structure is lowest for the cognate cases (Figure 3(b)). Average *B*-factors computed from the cognate UUU simulation are roughly consistent with those reported for the crystal structure, with the exception of 16 S rRNA base G1197 (Figure 3(c)). The similar results for UUU and UUC demonstrate the insensitivity of the simulation results to initial conditions.

Discrimination by minor groove measurement

In the cognate case, 16 S rRNA bases G530 and A1492 form an N1–H···N1 hydrogen bond across the minor groove of the codon–anticodon minihelix, shielding the codon–anticodon minor groove from solvent (Figure 4(a)). In the near-cognate UUA case, the tRNA–mRNA G34·A3 purine–purine mismatch sterically hinders the rRNA–rRNA G530·A1492 interaction, preventing the proper (i.e. cognate) hydrogen bond system from forming, while increasing the solvent exposure of the codon–anticodon pair (Figure 4(b)–(d)). In this sense, the 16 S rRNA pair G530·A1492 measures the depth of the codon–anticodon minor groove, consistent with the suggestion by Ramakrishnan and co-workers.[15]

To quantify the minor groove measurement mechanism, we examined the groove dimensions and hydrogen bond distances of the cognate UUU and near-cognate UUA systems. The difference in minor groove shape can be seen by comparing Figure 2(f) with Figure 4(d). The average groove depth for UUA is approximately 1.69 Å, significantly shallower than the UUU groove depth of 4.1 Å (Figure 4(c)). The shallower minor groove prevents the G530·A1492 N1–H···N1 hydrogen bond from forming, giving an average distance of 6.2 Å and N1–H···N1 angle of 75° for UUA, compared to an average distance of 2.0 Å and N1–H···N1 angle of 150° for UUU (Figure 4(c)). The groove width of UUA (11.1 Å) is similar to that of UUU (10.7 Å). The codon–anticodon base-pair hydrogen bonds for UUA are of comparable stability to the cognate case. That is, the distribution widths are similar, the D–H···A hydrogen bond distances are approximately 2.0 Å, and the D–H···A hydrogen bond angles are approximately 165°, where D corresponds to the donor and A to the acceptor. Thus, it is clear that the shallower minor groove of the UUA codon–anticodon minihelix and the strong stability of the G·A mismatch[36] contribute to the hindrance of the G530·A1492 interaction.

The steric hindrance of the rRNA G530·A1492 interaction results in a net loss of codon–anticodon–ribosome hydrogen bonds (Figure 3(a)), due to the repositioning of G530 and A1492 (Figure 4; UUA). The G530·A35 2′O–H···O2′ and A35·G530 2′O–H···N3 interactions do not form hydrogen bonds, displaying average D–H···A distances > 3.5 Å. Although there is a net loss of hydrogen bonds, the compensating interaction A1492·A36 N6–H···O2′ forms in approximately 42% of the configurations sampled, giving $N_H \cong 7.44$. The effect of codon–anticodon bases sterically hindering rRNA–rRNA interactions to produce an uncompensated loss of hydrogen bonds contrasts with the hypothesis that rRNA bases sterically hinder codon–anticodon interactions.[10] In addition to disturbing the codon–anticodon–ribosome hydrogen bonding network, the repositioning of G530 and A1492 also affects the solvent exposure of the codon–anticodon pair. Near-cognate minihelices have larger solvent accessible surface exposure compared to cognate minihelices. The average solvent accessible surface area, as calculated by the Maximal Speed Molecular Surface program,[37] for the UUU codon–anticodon–ribosome bases (i.e. mRNA bases U1, U2, and U3; tRNA bases G34, A35 and A36; and rRNA bases G530, A1492, and A1493) is approximately 2033 Å^2, while that of UUA is approximately 2080 Å^2.

Groove measurement allows the ribosome to distinguish between third position G·U wobbles and third position GA mismatches, which is essential for discrimination. Because the G530·A1492 and other cognate tRNA–rRNA interactions occur for the cognate case, but not for the near-cognate case, the scenario described above is consistent with discrimination by distortion detection.[9,10,15] In our simulations, steric effects and hydrogen bonding work together to distinguish between cognate and near-cognate interactions. The importance of the G530·A1492 interaction in discrimination is also consistent with the lethal mutation A1492G and the lethal mutation G530A, whose G·G and A·A clashes, respectively, would disrupt the G530·A1492 interaction, preventing proper

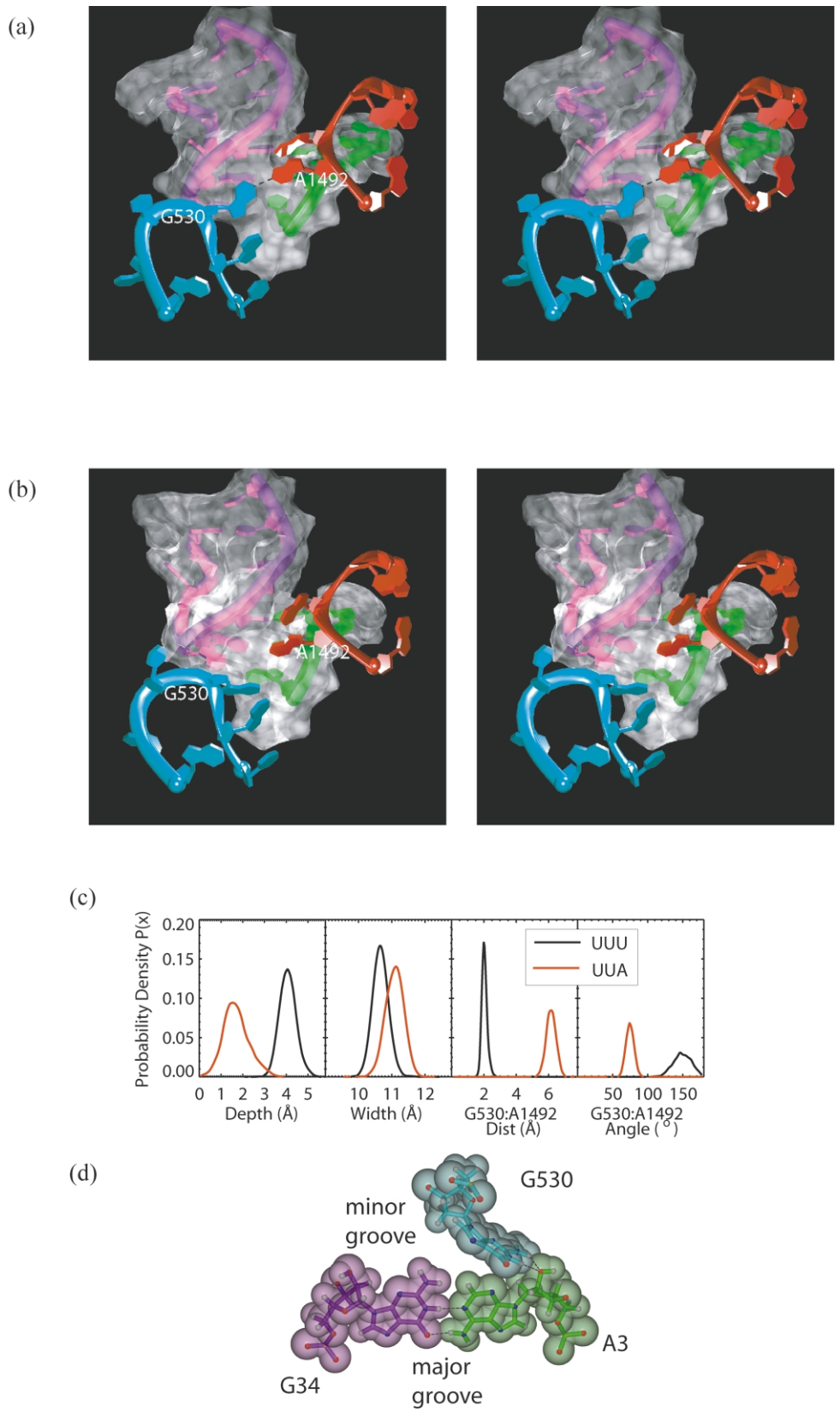

Figure 4. Measurement of the codon–anticodon minihelix minor groove by 16 S rRNA bases G530 and A1492. (a) and (b) The tRNA–ASL (purple) and messenger RNA (green) are shown beneath their transparent surfaces. Helix 44 (shown in red, including the flipped-out A1492 and A1493 bases) and 530 loop (shown in cyan, including *syn* to *anti* flipped G530 base) are shown in the foreground. (a) G530·A1492 N1–H ⋯ N1 interaction forms along the codon–anticodon minihelix minor groove for the cognate case. (b) The G530··A1492 interaction does not occur for the near-cognate case. (c) Probability distributions of the minor groove depth, width, and G530·A1492 N1–H···N1 hydrogen bond distance and angle for cognate and near-cognate simulations show that the near-cognate minor groove is not sufficiently deep to accommodate the G530·A1492 interaction. (d) The minor groove of the third position G·A mismatch for the near-cognate case has less room to accommodate 16 S rRNA base G530 compared to the cognate case (Figure 2(f)).

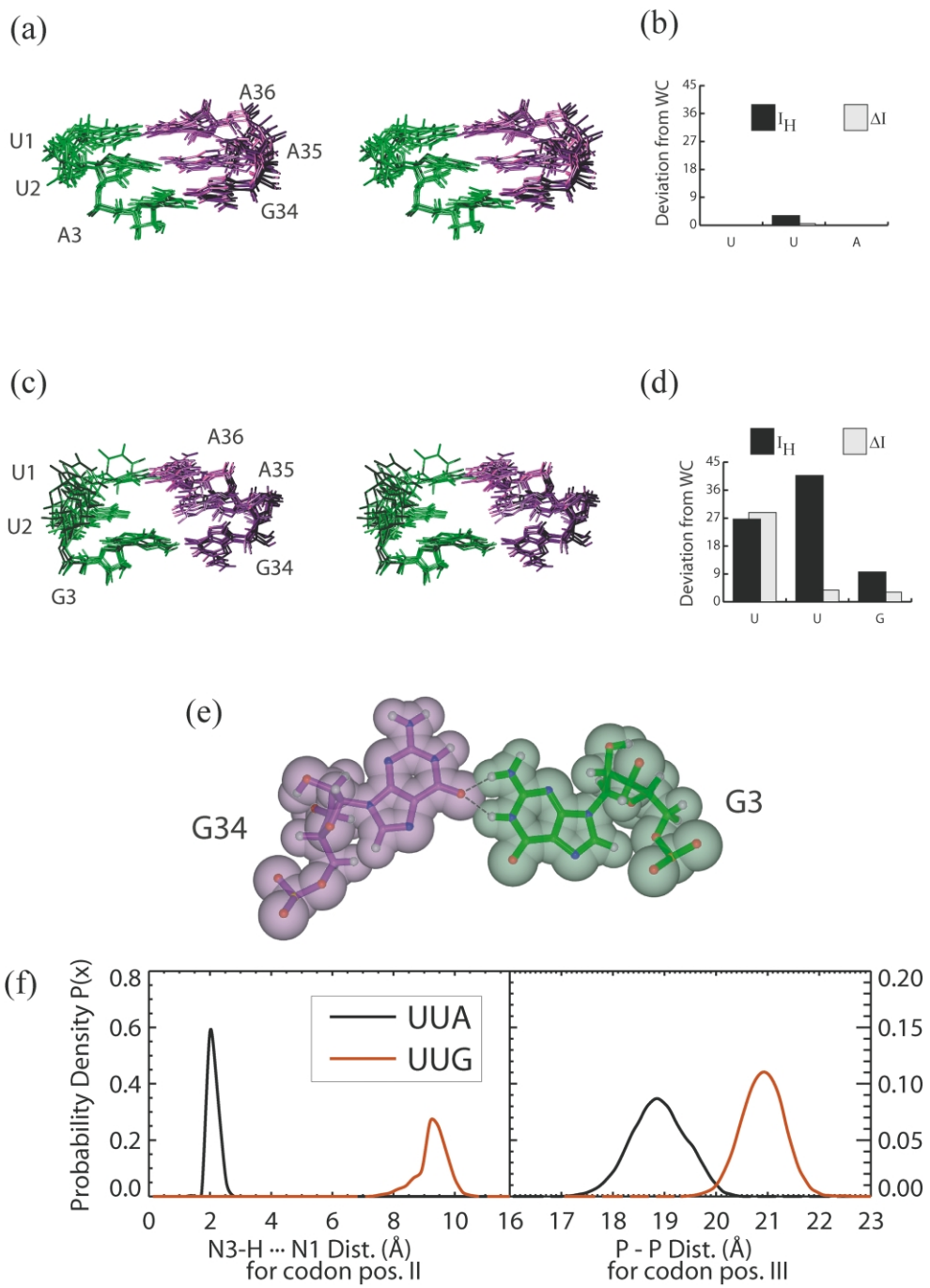

Figure 5. UUA has a third position G·A mismatch and is significantly more stable than UUG which has a third position G·G mismatch. (a) Superposition of five codon (green) anticodon (purple) structures taken at equally spaced intervals during the ribosomal decoding center simulation. (b) Quality index I_H of codon–anticodo-ribosome hydrogen bonds for each codon position shows relatively stable hydrogen bonds for UUA. (c) UUG displays large fluctuations and poor base-pair formation. (d) Quality indices for UUG show that the hydrogen bonds for UUG deviate significantly from those of Watson–Crick pairs. (e) UUG position III base-pair G3G34 displays the bifurcated hydrogen bond interaction N1–H···O6 and N2–H···O6. (f) Probability distributions for the second position base-pair hydrogen bond and the third position phosphate–phosphate distance. The wider position III phosphate–phosphate distance for UUG due to the G·G mismatch prevents the position II base-pair from forming.

discrimination.[38,39] However, it is possible that the double mutant A1492G·G530A may be viable because it preserves the N1–H···N1 interaction. The double mutant may be less functional than the wild-type because the A1492G base may have less tendency to flip out of helix 44, since this base will form a G·A pair with 16 S rRNA base A1408 in absence of A-tRNA as opposed to the less stable A·A pair which occurs in the wild-type structure.

Discrimination due to third position base-pair stability

While minor groove measurement distinguishes the near-cognate UUA from the cognate UUU, base-pair stability makes this distinction for the case of UUG. Our simulations show significantly different codon–anticodon–ribosome interactions for the UUG codon compared to those of UUA (Figure 5). While the UUA codon–anticodon base-pairs were quite stable (Figure 5(a),(b)), the UUG pairs produced poor hydrogen bond quality indices I_H (24-fold higher than UUA) and displayed high fluctuations ΔI_H (45-fold higher than UUA) (Figure 5(c),(d)). Because UUA and UUG differ in the third position only, the differences result from base-pair stability rather than mismatch position. The greater stability of UUA (third position G·A mismatch) compared to UUG (third position G·G mismatch) is consistent with thermal melting experiments, which rank G·A mismatches higher in stability than G·G mismatches.[36,40] G·A mismatches are higher in stability when compared to G·G mismatches, since G·A mismatches have a greater number of base-pair hydrogen bonds, as seen in Figures 4(d) and 5(e).

In the case of UUG, the G34·G3 base-pair interaction is skewed, resulting in the bifurcated hydrogen bond interaction, N1–H···O6 and N2–H···O6 (Figure 5(e)). This results in a position III (i.e. G34·G3) base-pair phosphate-phosphate distance of 20.91 Å (Figure 5(f)), larger than that of UUA (18.88 Å) and UUU (18.95 Å). The conformation of the G·G mismatch in position III prevents the position II A·U pair from forming base-pair hydrogen bonds, leaving a large gap between A35 and U2 (Figure 5(c)). The average U2·A35 N3–H···N1 distance is 9.3 Å for UUG, significantly wider that of UUA (2.1 Å) and UUU (2.0 Å) (Figure 5(f)). For UUG, only two (A36·A1493 2′O–H···N1; G3·G34 N1–H···O6) of the nine codon–anticodon–ribosome interactions form hydrogen bonds in more than 50% of the configurations sampled. The interaction G3·G34 N2–H···O6 also contributes to the average number of hydrogen bonds, giving in total $N_H \cong 4.89$. The wider G·G base-pair, combined with enhanced fluctuations due to the mRNA kink between A and P sites (discussed in detail below) results in large deviations from Watson–Crick geometry in all three codon–anticodon base-pairs.

Discrimination due to mRNA kink stability testing

To accommodate simultaneous codon–anticodon interactions in A and P sites, the mRNA has a significant kink between A and P sites[15,41] (Figure 1(d)). The non-helical structure of the mRNA kink prevents stacking interactions between mRNA bases N1 and U-1, giving the position I codon–anticodon base-pair (N1·A36) more room to fluctuate. Conversely, the position II base-pair (N2·A35) is stabilized by stacking interactions with the position I and position III base-pairs (N3·G34). As a result, our simulations show higher fluctuations at position I than position II (Figure 6). In Figure 6 we present results for the cognate UUU system, the near-cognate CUC system (position I C·A mismatch), and the near-cognate UCU system (position II C·A mismatch). While the cognate UUU first position codon–anticodon pair (U1·A36) remains stable (Figure 6(a),(b)), the near-cognate CUC first position pair (C1·A36) is disrupted (Figure 6(c),(d)), producing a position I quality index approximately fourfold higher than the UUU position I index. Here, base-pairs which are normally more stable in a duplex are not stable when adjacent to a kink, where they are more exposed to solvent and do not participate in strong stacking interactions. In this sense, the mRNA kink between A and P sites tests the stability of the position I base-pair. The CUC codon–anticodon complex has an additional hydrogen bond due the G34·C3 Watson–Crick pair; however, the position I fluctuations disrupt the interaction A36·A1493 2′O–H···N1, in addition to the position I base-pair bonds, giving $N_H \cong 7.32$.

For the UCU near-cognate simulation, severe disruptions in both the first and second position base-pairs were observed, evidenced by the poor base-pair quality index, and absence of several hydrogen bonds in positions I and II (Figure 6(e),(f)). The deviation from Watson–Crick is more than ninefold higher for UCU relative to CUC at position I and more than 40-fold higher at position II. In this case, the non-ideal geometry of the position II C·A base-pair (Figure 6(g)) exerts a strain on the first position base-pair. This, in combination with the mRNA kink and perturbation by A1493 (discussed in detail in the next section), is sufficient to disrupt the Watson–Crick base-pair in position I, in addition to the non-Watson–Crick base-pair in position II. Thus, in a similar manner to the destabilization of the UUG system, stress due to the mismatch geometry, the mRNA kink and perturbation by A1493 combine to test the strength of the codon–anticodon–ribosome hydrogen bond network. In this case, no tRNA–ASL interactions involving the ribosome form stable hydrogen bonds. Only the A35·C2 and G34·U3 interactions form hydrogen bonds in more than 50% of the configurations. The other codon–anticodon–ribosome interactions are extremely weak and transient for this case, but do contribute to the average number of hydrogen bonds, giving in total $N_H \cong 4.61$.

For each of the above cases, fluctuations in position III ($\Delta I_H \sim 0.03$) are markedly lower than those in position II ($\Delta I_H > 0.2$) and position I ($\Delta I_H > 0.4$). This results from stabilization by 16 S rRNA base C1054, which forms a strong stacking interaction with G34 (Figure 6(a)), while simultaneously forming a hydrogen bond with U4 (C1054·U4 N4–H···O2) (Figure 6(h)). These interactions are observed for many of the codons

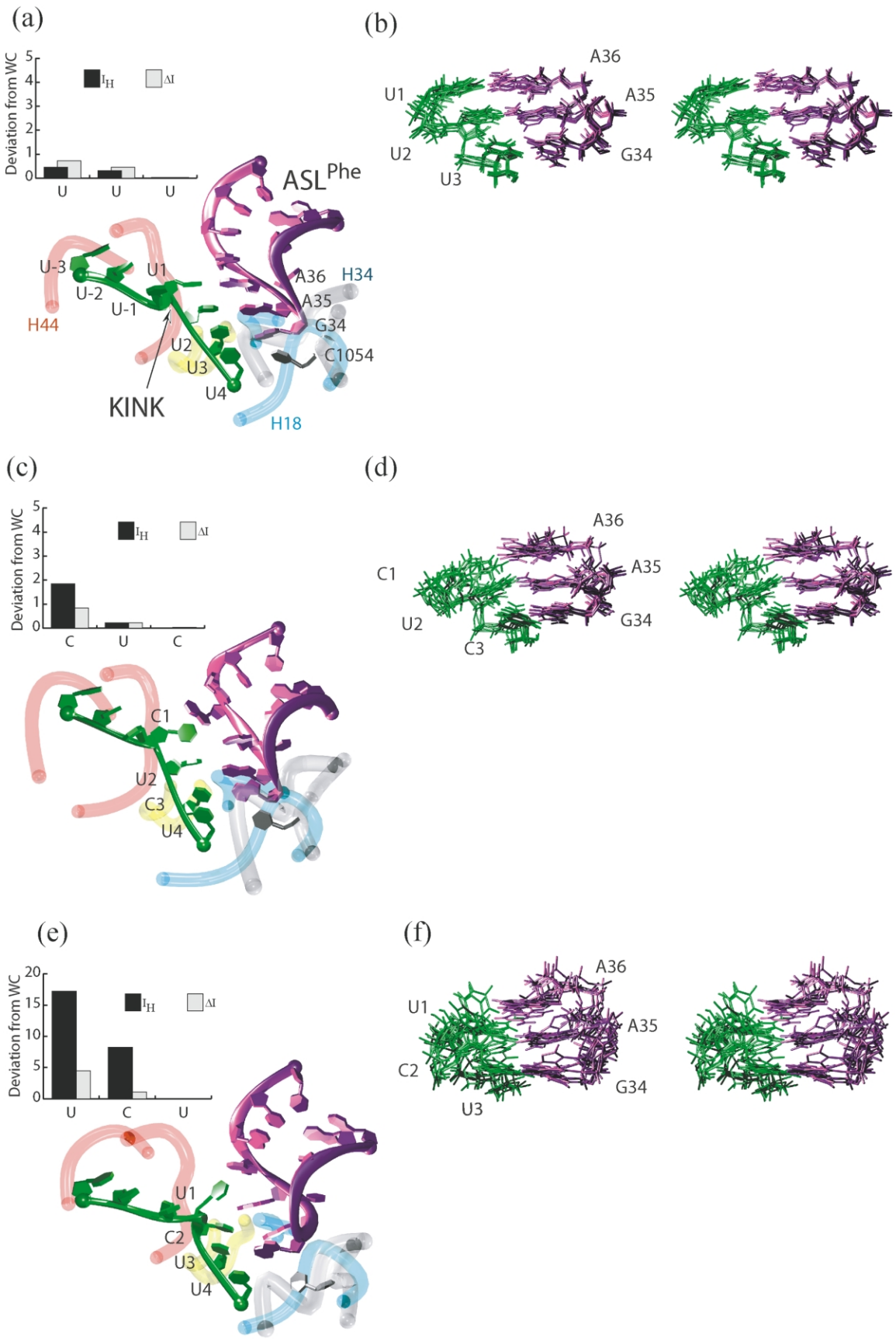

Figure 6 (*legend opposite*)

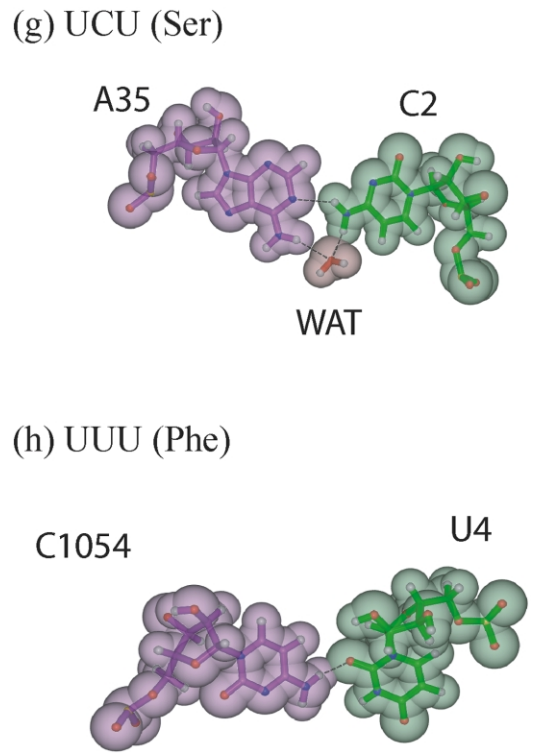

Figure 6. The mRNA kink between A and P sites exposes the position I A-site codon–anticodon base-pair to larger fluctuations relative to positions II and III. (a) Configuration of the simulation domain for the cognate UUU (Phe) case at 3.0 ns. Bases are shown for the mRNA and tRNA. Only the backbone is shown for H44 (red), S12 (yellow), H18 (cyan), and H34 (grey). Water is not shown. The hydrogen bond quality indices (I_H) and their fluctuations (ΔI_H) indicate stable codon–anticodon hydrogen bonds (inset). (b) Superposition of five UUU configurations taken at equally spaced times during the simulation exhibit stable codon–anticodon interactions. (c) The near-cognate case CUC (Leu) shows significant deviation from Watson–Crick in the first codon position, adjacent to the mRNA kink. (d) The near-cognate case CUC (Leu) shows larger fluctuations than the cognate UUU (Phe) case. (e) The near-cognate case UCU (Ser) shows a large deviation, with many codon–anticodon–ribosome hydrogen bonds disrupted. The largest disruptions occur in the first codon position, adjacent to the kink. (f) Configurations of UCU (Ser) show larger fluctuations than CUC (Leu) and UUU (Phe). (g) UCU position II C2·A35 mismatch displays the water-mediated interaction A35·WAT·C2 N6–H···O_{HOH}···H–N4. (h) The C1054·U4 interaction N4–H···O2 stabilizes the position III G34·U3 pair for the cognate (displayed) and many near-cognate cases (not shown).

simulated and present an obvious mechanism for maintaining the reading frame.[42] The accepting partner of the hydrogen bond (O2) is sequence-independent in the same sense that the A1493·U1 2′O–H···O2 hydrogen bond is sequence independent, as argued by Ogle *et al*.[15]

The stability testing by the kink in mRNA between A and P sites is a logical consequence of the X-ray structure and provides an efficient method of ordering of position-dependent destabilization. While codons with non-GA mismatches in the first position suffer one disrupted base-pair, those with non-GA mismatches in the second position suffer two disrupted base-pairs. The severe disruption of second position mismatches is consistent with the infrequent occurrence of errors (due to a high rate of rejection) in codon position II relative to codon position I for codon–anticodon pairs with C·A and A·A mismatches.[3,43]

Destabilization by the ribosome

To further investigate the role of the ribosome, simulations for the UCU case were repeated without any ribosomal RNA or protein. The ASL^{Phe} and mRNA were simulated with the same geometry and restraints, enabling us to compare the codon–anticodon stability with and without ribosomal bases. In the absence of the ribosome, the base-pair fluctuations were markedly lower (Figure 7(a),(b)). The fluctuations and quality indices are more than an order of magnitude lower in the UCU simulation without the ribosome (Figure 7(b)) than the UCU simulation with the ribosome (Figure 6(e), inset). The relative stability of the codon–anticodon minihelix for UCU in absence of the ribosome contrasts with the disruption of the first and second position base-pairs in the presence of the ribosome, suggesting that the ribosome interferes with near-cognate UCU codon–anticodon pairing.

Upon close inspection of the simulation trajectories, 16 S rRNA base A1493 was observed to perturb the ribose of codon base U1. In particular, the 2′OH and 4′C–H groups of A1493 compete with each other for an interaction with the 2′O of U1, enhancing the fluctuations of the U1 ribose.[44–46] This competition results from the water-mediated C2·A35 pair (Figure 6(g)) which alters the minihelix conformation to expose the 2′O of U1 to the 4′C–H of A1493. The C2·A35 pair has one base-pair hydrogen bond (N4–H···N1) and one water-mediated interaction (A35·WAT·C2 N6–H···O_{WAT}···H–N4), and happens to be the most common C·A pair configuration in the 23 S subunit.[47] The water-mediated configuration of the second position C·A base-pair works in concert with the perturbation by A1493 and enhanced fluctuations due to the mRNA kink to disrupt the UCU minihelix. The perturbation by A1493 did not occur in our simulation without the ribosome, resulting in significantly more stable codon–anticodon base-pairs. Thus, the decoding base A1493 enhances stability differences by stabilizing cognate codon–anticodon pairs while destabilizing near-cognate codon–anticodon pairs, consistent with suggestions that the ribosome amplifies codon–anticodon stability differences.[23,24]

Conclusions

Groove measurement by the interaction between 16 S rRNA bases G530 and A1492 allows the

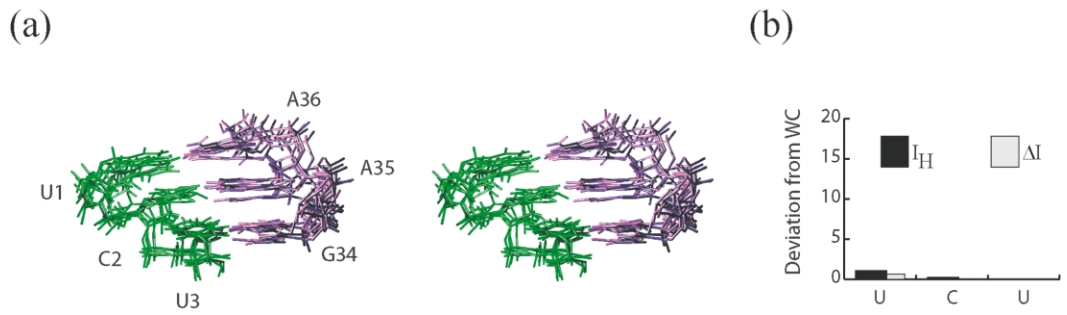

Figure 7. (a and b) Simulations of UCU (Ser) without the ribosome, but with the same mRNA–tRNA geometry. (a) Five superimposed configurations taken at equally spaced intervals in the UCU simulation without the ribosome. (b) The corresponding quality indices (I_H) and their fluctuations (ΔI_H). Comparison with Figure 6(e), inset (UCU with ribosome),suggests that the ribosome destabilizes the codon–anticodon interactions for the case of UCU.

ribosome to distinguish between cognate and near-cognate codon–anticodon pairs which are similar in stability, yet different in shape (i.e. near-cognates containing a G·A purine–purine mismatch). Stability testing by the mRNA kink and by 16 S rRNA base A1493 enable the ribosome to distinguish between cognate and near-cognate codon–anticodon pairs which are similar in shape (i.e. contain only purine–pyrimidine pairs), yet different in stability. Thus, for certain near-cognates, discrimination occurs through a combination of steric fit and hydrogen bond reorganization, while for other cases, base-pair stability is used. Additionally, stability testing by the mRNA kink provides position-dependent discrimination, destabilizing codon–anticodon pairs with position II mismatches more severely than those with position I mismatches, consistent with the positional dependence of discrimination rates.[3,43] These simulations have allowed to us make the predictions that: (1) for the case of $tRNA^{Phe}$, the near-cognate codon UUA should display more stable codon–anticodon–ribosome interactions than the near-cognate codon UUG; and (2) the double mutation G530A·A1492G should be viable.

Because the discrimination effects observed in our simulations are independent of the 50 S subunit and of regions on the 30 S subunit outside of the decoding center, our results support the integrated view of the decoding mechanism, where GTPase activation and accommodation occur as a concerted process.[14] During GTPase activation, a signal must be communicated from the decoding center to the elongation factor EF-Tu. This signal may be sent from the 30 S to the 50 S *via* the conformational change of the 30 S or, as recently suggested, by the tRNA itself.[17] Strong hydrogen bonding of 16 S rRNA bases A1492, A1493 and G530 to the codon and anticodon bases is required to shift the conformation equilibrium of these bases from the flipped-in to flipped-out conformation (A1492,A1493) and from the *syn* to *anti* conformation (G530). Shifting this equilibrium may stabilize the closed conformation of the 30 S small subunit, which in turn will perturb the conformation of the 50 S subunit. Our simulations exhibit stronger hydrogen bonding both in the form of more stable hydrogen bonds and a greater number of hydrogen bonds for cognate cases relative to near-cognate cases. With regard to signal communication *via* the tRNA, although the tRNA is quite flexible, the orientation of the acceptor stem is not independent of the orientation of the ASL. There must be an optimal orientation for the ASL portion of the tRNA at the decoding site to achieve efficient rates of GTP hydrolysis. In our simulations, the near-cognate ASLs are significantly misaligned when compared to cognate ASLs as a result of the disrupted codon–anticodon–ribosome hydrogen bond network. To explore these issues in more detail, a simulation of the 70 S ribosome must be performed.

The stability testing and groove measurement discrimination effects described here rely on universally conserved 16 S rRNA bases and on the highly conserved tertiary structure of tRNA, suggesting that the mechanisms themselves may be highly conserved. A system of simultaneous and in some cases redundant checks, as suggested by our simulations, may be necessary to ensure the high level of fidelity required for accurate protein synthesis.

Methods

Molecular dynamics simulations

The systems were advanced in time with the Cornell *et al*. force field PARM94[48] and the AMBER 6.0 suite of simulation codes,[49] using the particle-mesh Ewald option. SHAKE was used to constrain bonds involving hydrogen. Integration was performed with the Berendsen algorithms (used to couple to the system to an external heat bath)[50] using $\tau_T = 0.2$ ps and a time step of 2 fs. Approximately 6×10^4 CPU hours were used on a LINUX cluster.

System setup

The initial configuration of the decoding center of the 30 S subunit complexed with ASL^{Phe} and cognate mRNA analog was taken directly from the X-ray

structure (RCSB PDB accession code 1IBM).[15] The simulation domain included ASL^{Phe}, the seven base mRNA fragment, stretches of helix 44, helix 34, helix 18 and ribosomal protein S12. This amounted to 54 nucleotides and nine amino acid residues. The size of the simulation domain was chosen to capture all direct codon–anticodon–ribosome interactions as well as important indirect interactions. For example, both strands of helix 44 were included even though only one strand directly interacts with the codon–anticodon helix. The cognate seven base mRNA fragment (5′-UCUUUUU-3′) was created by ligating the UCU and UUUU fragments present in the X-ray structure (RCSB PDB accession code 1IBM). The joining phosphate group was fit to the mRNA of Protein Data Bank structure 1GIX.[41] This was subsequently minimized and equilibrated (see below). The near-cognate mRNA codons were created by replacing one base in the A site mRNA codon and subsequently minimizing and equilibrating (see below). The systems were neutralized with 44 sodium ions placed at electrostatic potential minima. The systems were then solvated with approximately 7×10^3 water molecules, using the Tip3p water model.[48]

Minimization and equilibration

The solvent was minimized using steepest descent minimization for 1000 steps, while the solute atoms were fixed in space. Subsequently, the solute and solvent were minimized for 1000 steps. The solvent was then subjected to 10 ps of molecular dynamics simulation at $T = 10$ K and constant (N, P, T), during which the solute was restrained by a harmonic potential of 200 kcal/mol Å^2. Over the next 36 ps, the potential was gradually lowered to zero while the temperature was increased from 10 K to 300 K. The nucleotides at the 5′ and 3′ ends of the rRNA fragments (with the exception of the tRNA anticodon stem-loop) and the residues at the C and N termini of S12 were restrained by a harmonic potential of 8 kcal/mol Å^2. The mRNA base to the 3′ side of the A site codon (U4 of Figure 1(c)) was restrained by a weaker harmonic potential of 2.5 kcal/mol Å^2. The P site mRNA codon was also restrained to emulate the presence of a P site tRNA. However, the restraint was gradually tapered off to avoid artificially high bending stress between A and P site codons. That is, U-3 (Figure 1(a)) was restrained at 8 kcal/mol Å^2, U-2 was restrained at 2.5 kcal/mol Å^2 and U-1 was unrestrained. Equilibration was then performed at 300 K and constant (N, V, T) giving a total equilibration time of 770 ps.

Because restraints are used the system does not display center of mass motion nor overall rotation.[51]

Post-simulation analysis

Figures were created with IDL, POV-Ray, MOLMOL[52] and DINO.[53] Probability densities were normalized to the number of bins in the x-axis domain. The minor groove depth was calculated using a similar method described by Bhattacharyya & Bansal.[54] Distributions were determined from the later 2296 ps of the simulations and were smoothed using hanning[55] and B-spline[56] smoothing. D–H···A interactions with distances less than 2.65 Å and angles greater than 120° were considered hydrogen bonds, consistent with the results described by Ogle *et al*.[15] The number of hydrogen bonds is represented by $N_H = \sum N_i/N_{tot}$, where N_i represents the total number of codon–anticodon–ribosome hydrogen bond interactions satisfying the above criterion for the ith configuration, N_{tot} the total number of post-equilibration configurations, and $i = 1,\ldots, N_{tot}$. Average solvent accessible surface areas were calculated with the Maximal Speed Molecular Surface program (MSMS).[37] B-factors were calculated using RMSD values from the simulation. The curve of B-factor *verses* nucleotide number was subsequently fit to that of the X-ray structure using the bases which were restrained in the simulation in order to compensate for the use of positional restraints in the simulation. The level of fluctuations is described by the dimensionless hydrogen bond quality index, $I_H = \sum (d_j - d_0)^2/a^2 + (1 + \cos \gamma_j)^2$, where d_j is the D–H···A atom distance, γ_j is the D–H···A angle, $d_0 = 1.9$ Å, and $a = 1$ Å.[57] The index j is summed over those codon–anticodon–ribosome hydrogen bonds involving the tRNA–ASL. The quality index I_H is a measure of the deviation from Watson–Crick hydrogen bond geometry in the sense that $I_H = 0$ for hydrogen bond distances and angles corresponding to ideal Watson–Crick hydrogen bonds (i.e. $d_j = d_0$ and $\gamma_j = 180°$). The cognate cases, which display the most stable hydrogen bonds, have an average hydrogen bond distance of 2.1 Å with a standard deviation of 0.25 Å and an average angle of 156° with a standard deviation of 14°. Using bond values one standard deviation away from the cognate value (i.e. $d_j = 2.35$ Å and $\gamma_j = 141°$), the quality index is $I_H = 0.25$. Thus, for $I_H \gg 0.25$, the hydrogen bonds deviate significantly from a Watson–Crick hydrogen bond. The values reported for I_H are averaged over all post-equilibration configurations. The standard deviation of the distribution of I_H values is represented by ΔI_H.

Sensitivity to initial conditions and simulation parameters

Simulations performed with significantly larger ribosomal domains (36,000 atoms) gave qualitatively similar results and demonstrated that the codon–anticodon interaction is not significantly affected by including this larger region of the decoding center. Simulations including 16 S rRNA bases 912–916 and 1395–1404 (in addition to the domain displayed in Figure 1(b)) displayed stable codon–anticodon interactions for UUU and unstable interactions for UCU in a manner similar to that described above. Control simulations were also performed using potassium counter ions rather than sodium counter ions. This did not effect the codon–anticodon interaction significantly. The kink effect is robust in the sense that higher fluctuations in the position I base-pair occurred for all near-cognate cases with non-GA mismatches in first or second positions (CUC, CUU, AUU, UCU, and UAU). Those near-cognates with first position non-GA mismatches behave similarly (CUC, CUU, and AUU). Near-cognates with second position non-GA mismatches also behaved similarly (UCU and UAU). Both cognate cases (UUU and UUC) exhibited significantly more stable interactions.

Acknowledgements

This work was performed under the auspices of the United States Department of Energy. K.Y.S. is supported by grants from the LANL/LDRD

program. S.J. is supported by NSF and NIH grants. This work benefited from useful discussions with V. Ramakrishnan, J. Frank, J. Hopfield, K. Nierhaus, E. Westhof, M. Rodnina, H. F. Noller, A. E. Garcia, and C. S. Tung.

References

1. Gilbert, W. (1963). Polypeptide synthesis in Escherichia coli. *J. Mol. Biol.* **6**, 389–403.
2. Watson, J. D. (1963). Involvement of RNA in the synthesis of proteins. *Science*, **140**, 17–26.
3. Davies, J., Gilbert, W. & Gorini, L. (1964). Streptomycin, suppression and the code. *Biochemistry*, **51**, 883–890.
4. Rodnina, M. V. & Wintermeyer, W. (2001). Fidelity of aminoacyl-tRNA selection on the ribosome: Kinetic and structural mechanisms. *Annu. Rev. Biochem.* **70**, 415–435.
5. Ninio, J. (1974). A semi-quantitative treatment of missense and nonsense suppression in the strA and ram ribosomal mutants of Escherichia coli: Evaluation of some molecular parameters of translation *in vivo*. *J. Mol. Biol.* **84**, 297–313.
6. Hopfield, J. J. (1974). Kinetic Proofreading: New Mechanism for Reducing Errors in Biosynthetic Processes Requiring High Specificity. *Proc. Natl Acad. Sci. USA*, **71**, 4135–4139.
7. Thompson, R. C. & Stone, P. J. (1977). Proofreading of codon–anticodon Interaction on Ribosomes. *Proc. Natl Acad. Sci. USA*, **74**, 198–202.
8. Pape, T., Wintermeyer, W. & Rodnina, M. (1999). Induced fit in initial selection and proofreading of aminoacyl-tRNA on the ribosome. *EMBO J.* **18**, 3800–3807.
9. Potapov, A. P., Trianaalonso, F. J. & Nierhaus, K. H. (1995). Ribosomal Decoding Processes at Codons in the a-Site or P-Site Depend Differently on 2(-Oh Groups. *J. Biolo. Chem.* **270**, 17680–17684.
10. Lim, V. I. & Curran, J. F. (2001). Analysis of codon: anticodon interactions within the ribosome provides new insights into codon reading and the genetic code structure. *RNA—a publication of the RNA society*, **7**, 942–957.
11. Nierhaus, K. H. (1990). The Allosteric 3-Site Model for the Ribosomal Elongation Cycle: Features and Future. *Biochemistry*, **29**, 4997–5008.
12. Blaha, G. & Nierhaus, K. H. (2001). *Features and functions of the ribosomal E site* Cold Spring Harbor Symposia on Quantitative Biology LXVI: The Ribosome, vol. 66, Cold Spring Harbor Laboratory Press, Cold Spring Harbor pp. 135–146.
13. Ramakrishnan, V. (2002). Ribosome structure and the mechanism of translation. *Cell*, **108**, 557–572.
14. Ogle, J. M., Murphy, F. V., Tarry, M. J. & Ramakrishnan, V. (2002). Selection of tRNA by the ribosome requires a transition from an open to a closed form. *Cell*, **111**, 721–732.
15. Ogle, J. M., Brodersen, D. E., Clemons, W. M., Tarry, M. J., Carter, A. P. & Ramakrishnan, V. (2001). Recognition of cognate transfer RNA by the 30S ribosomal subunit. *Science*, **292**, 897–902.
16. Broderson, D. E., Carter, A. P., Clemmons, W. M., Morgan-Warren, R. J., Murphy, F. V., Ogle, J. M., *et al.* (2001). *Atomic structures of the 30S subunit and its complexes with ligands and antibiotics* Cold Spring Harbor Symposia on Quantitative Biology LXVI: The Ribosome, vol. 66, Cold Spring Harbor Press, Cold Spring Harbor pp. 17–32.
17. Valle, M., Sengupta, J., Swami, N. K., Grassucci, R. A., Burkhardt, N., Nierhaus, K. H. *et al.* (2002). Cryo-EM reveals an active role for aminoacyl-tRNA in the accommodation process. *EMBO J.* **21**, 3557–3567.
18. Stark, H., Rodnina, M. V., RinkeAppel, J., Brimacombe, R., Wintermeyer, W. & vanHeel, M. (1997). Visualization of elongation factor Tu on the Escherichia coli ribosome. *Nature*, **389**, 403–406.
19. Lodmell, J. S. & Dahlberg, A. E. (1997). A conformational switch in Escherichia coli 16S ribosomal RNA during decoding of messenger RNA. *Science*, **277**, 1262–1267.
20. Powers, T. & Noller, H. F. (1994). Selective Perturbation of G530 of 16 S-Ribosomal-RNA by Translational Miscoding Agents and a Streptomycin-Dependence Mutation in Protein-S12. *J. Mol. Biol.* **235**, 156–172.
21. Kurland, C. G., Rigler, R., Ehrenberg, M. & Blomberg, C. (1975). Allosteric Mechanism for Codon-Dependent Transfer-RNA Selection on Ribosomes. *Proc. Natil Acad. Sci. USA*, **72**, 4248–4251.
22. Kurland, C. G. (1992). Translational accuracy and the fitness of bacteria. *Annu. Rev. Genet.* **26**, 29–50.
23. Thompson, R. C. & Dix, D. B. (1982). Accuracy of Protein-Biosynthesis: A Kinetic-Study of the Reaction of Poly(U)-Programmed Ribosomes with a Leucyl-Transfer RNA2-Elongation Factor Tu-GTP Complex. *J. Biol. Chem.* **257**, 6677–6682.
24. Grosjean, H. J., Dehenau, S. & Crothers, D. M. (1978). Physical Basis for Ambiguity in Genetic Coding Interactions. *Proc. Natl Acad. Sci. USA*, **75**, 610–614.
25. Karplus, M. & McCammon, J. A. (2002). Molecular dynamics simulations of biomolecules. *Nature Struct. Biol.* **9**, 646–652.
26. Berneche, S. & Roux, B. (2001). Energetics of ion conduction through the K + channel. *Nature*, **414**, 73–77.
27. Bockmann, R. A. & Grubmuller, H. (2002). Nanoseconds molecular dynamics simulation of primary mechanical energy transfer steps in F1-ATP synthase. *Nature Struct. Biol.* **9**, 198–202.
28. Young, M. A., Gonfloni, S., Superti-Furga, G., Roux, B. & Kuriyan, J. (2001). Dynamic coupling between the SH2 and SH3 domains of c-Src and Hck underlies their inactivation by C-terminal tyrosine phosphorylation. *Cell*, **105**, 115–126.
29. Tajkhorshid, E., Nollert, P., Jensen, M. O., Miercke, L. J., O'Connell, J., Stroud, R. M. & Schulten, K. (2002). Control of the selectivity of the aquaporin water channel family by global orientational tuning. *Science*, **296**, 525–530.
30. Sporlein, S. H. C., Satzger, H., Renner, C., Behrendt, R., Moroder, L., Tavan, P. *et al.* (2002). Ultrafast spectroscopy reveals subnanosecond peptide conformational dynamics and validates molecular dynamics simulation. *Proc. Natl Acad. Sci. USA*, **99**, 7998–8002.
31. Cheatham, T. E. & Kollman, P. A. (2000). Molecular dynamics simulation of nucleic acids. *Annu. Rev. Phys. Chem.* **51**, 435–471.
32. Auffinger, P. & Westhof, E. (2000). Water and ion binding around RNA and DNA (C;G) oligomers. *J. Mol. Biol.* **300**, 1113–1131.
33. VanLoock, M. S., Easterwood, T. R. & Harvey, S. C. (1999). Major groove binding of the tRNA/mRNA complex to the 16 S ribosomal RNA decoding site. *J. Mol. Biol.* **285**, 2069–2078.

34. Simonson, A. B. & Lake, J. A. (2002). The trans-orientation hypothesis for codon recognition during protein synthesis. *Nature*, **416**, 281–285.
35. Lahiri, A. & Nilsson, L. (2000). Molecular dynamics of the anticodon domain of yeast tRNA(Phe): codon–anticodon interaction. *Biophys. J.* **79**, 2276–2289.
36. Turner, D. H. (1996). Thermodynamics of base pairing. *Curr. Opin. Struct. Biol.* **6**, 299–304.
37. Sanner, M., Olson, A. J. & Spehner, J. C. (1996). Reduced surface: an efficient way to compute molecular surfaces. *Biopolymers*, **38**, 305–320.
38. Powers, T. & Noller, H. F. (1990). Dominant lethal mutations in a conserved loop in 16 S ribosomal-RNA. *Proc. Natl Acad. Sci. USA*, **87**, 1042–1046.
39. Yoshizawa, S., Fourmy, D. & Puglisi, J. D. (1999). Recognition of the codon–anticodon helix by ribosomal RNA. *Science*, **285**, 1722–1725.
40. Gautheret, D. F., Konings, D. & Gutell, R. R. (1994). A Major Family of Motifs Involving GA Mismatches in Ribosomal-RNA. *J. Mol. Biol.* **242**, 1–8.
41. Yusupov, M. M., Yusupova, G. Z., Baucom, A., Lieberman, K., Earnest, T. N., Cate, J. H. D. & Noller, H. F. (2001). Crystal structure of the ribosome at 5.5 angstrom resolution. *Science*, **292**, 883–896.
42. Stahl, G., McCarthy, G. P. & Farabaugh, P. J. (2002). Ribosome structure: revisiting the connection between translational accuracy and unconventional decoding. *Trends Biochem. Sci.* **26**, 178–183.
43. Parker, J. (1989). Errors and Alternatives in Reading the Universal Genetic-Code. *Microbiol. Rev.* **53**, 273–298.
44. Taylor, R. & Kennard, O. (1982). Crystallographic evidence of the existence of C-H−-O, C-H−-N, and C-H−-Cl hydrogen bonds. *J. Am. Chem. Soc.* **104**, 5063–5070.
45. Jeffrey, G. A. (1989). Hydrogen-bonding in crystal structures of nucleic acid components: purines, pyrimidines, nucleosides and nucleotides. In *Numerical Data and Functional Relationships in Science and Technology* (Saenger, W., ed.), pp. 277–348, Springer, Berlin.
46. Jeffrey, G. A. (1997). *An introduction to hydrogen bonding*, Oxford University Press, Oxford.
47. Nagaswamy, U., Lorios-Sanz, M., Hury, J., Collins, S., Zhang, Z. D., Zhao, Q., Fox, G. E. & NCIR:, A. (2002). database of non-canonical interactions found in known RNA structures. *Nucl. Acids Res.* **30**, 395–397.
48. Cornell, W. D., Cieplak, P., Bayly, C. I., Gould, I. R., Merz, K. M., Ferguson, D. M. *et al.* (1995). A 2nd Generation Force-Field for the Simulation of Proteins; Nucleic-Acids; and Organic-Molecules. *J. Am. Chem. Soc.* **117**, 5179–5197.
49. Pearlman, D. A., Case, D. A., Caldwell, J. W., Ross, W. S., Cheatham, T. E., Ferguson, D. M., *et al.* (1994). *AMBER*, 4.1 edit., University of California, San Francisco.
50. Berendsen, H. J. C., Postma, J. P. M., Vangunsteren, W. F., Dinola, A. & Haak, J. R. (1984). Molecular-Dynamics with Coupling to an External Bath. *J. Chem. Phys.* **81**, 3684–3690.
51. Harvey, S. C., Tan, R. K. Z. & Cheatham, T. E. (1998). The flying ice cube: Velocity rescaling in molecular dynamics leads to violation of energy equipartition. *J. Comput. Chem.* **19**, 726–740.
52. Koradi, R., Billeter, M. & Wuthrich, K. (1996). MOLMOL: a program for display and analysis of macromolecular structures. *J. Mol. Graph.* **14**, 51–55.
53. Philippsen, A., (2002). DINO 0.8 edit. Division of Structural Biology, Biozentrum, University of Basel, Switzerland.
54. Bhattachary, D. & Bansal, M. (1992). Groove width and depth of B-DNA structures depend on local variation in slide. *J. Biomol. Struct. Dynam.* **10**, 213–226.
55. Press, W. H., Teukolsky, S. A., Vetterling, W. T. & Flannery, B. P. (1992). *Numerical Recipes in Fortran 77 Second Edition*, Cambridge University Press, Cambridge, UK.
56. de Boor, C. (1977). Package for calculating with B-splines. *SIAM J. Numerical Anal.* **14**, 441–472.
57. Yan, S., Shapiro, R., Geacintov, N. E. & Broyde, S. (2001). Stereochemical, structural, and thermodynamics origins of stability differences between stereoisomeric Benzoa.pyrene Diol Epoxide Deoxyadenosine adducts in a DNA mutational hot spot sequence. *J. Am. Chem. Soc.* **123**, 7054–7066.
58. Nissen, P., Ippolito, J. A., Ban, N., Moore, P. B. & Steitz, T. A. (2001). RNA tertiary interactions in the large ribosomal subunit: The A-minor motif. *Proc. Natl Acad. Sci. USA*, **98**, 4899–4903.
59. Doherty, E. A., Batey, R. T., Masquida, B. & Doudna, J. A. (2001). A universal model of helix packing in RNA. *Nature Struct. Biol.* **8**, 339–343.

Edited by D. E. Draper

(Received 14 October 2002; received in revised form 10 February 2003; accepted 11 February 2003)